HHS Public Access

Author manuscript

Chem Eng J. Author manuscript; available in PMC 2019 December 01.

Published in final edited form as:

Chem Eng J. 2018 December 1; 353: 657–665. doi:10.1016/j.cej.2018.07.124.

Insight on the generation of reactive oxygen species in the CaO_2/Fe(II) Fenton system and the hydroxyl radical advancing strategy

Yunfei Xue[a,b], **Qian Sui**[a,b,*], **Mark L. Brusseau**[c], **Xiang Zhang**[a], **Zhaofu Qiu**[a], **Shuguang Lyu**[a,b,*]

[a]State Environmental Protection Key Laboratory of Environmental Risk Assessment and Control on Chemical Process, East China University of Science and Technology, Shanghai 200237, China;

[b]Shanghai Institute of Pollution Control and Ecological Security, Shanghai 200092, China;

[c]Soil, Water and Environmental Science Department, School of Earth and Environmental Sciences, The University of Arizona, Tucson, AZ 85721, United States;

Abstract

Calcium peroxide (CaO_2) is a stable hydrogen peroxide (H_2O_2) carrier, and the CaO_2/Fe(II) system has been applied for treatment of various pollutants. It is commonly reported in the literature that hydroxyl radical ($HO^{\bullet}$) and superoxide radical anions ($O_2^{\bullet-}$) are the two main reactive oxygen species (ROSs) generated in the CaO_2/Fe(II) system. However, many of the reported results were deduced from degradation performance rather than specific testing of radical generation. Thus, the specific generation of ROSs and the influence of system conditions on ROSs yield is still unclear. To our knowledge, this is the first study specifically focusing on the generation of $HO^{\bullet}$ and $O_2^{\bullet-}$ in the CaO_2/Fe(II) system. Experimental conditions were optimized to investigate the production of $HO^{\bullet}$ and $O_2^{\bullet-}$. The results showed the influences of CaO_2, Fe(II), and solution pH on $HO^{\bullet}$ and $O_2^{\bullet-}$ generation, and the $HO^{\bullet}$ generation efficiency was reported for the first time. In addition, the ROSs generation pathways in the CaO_2/Fe(II) system were elucidated. A strategy for enhancing $HO^{\bullet}$ yield is developed, based on the continuously dosing Fe(II). This proposed strategy has implications for the effective application of *in situ* chemical oxidation employing CaO_2/Fe(II) for groundwater remediation.

Keywords

Hydroxyl radical; Superoxide radical anion; CaO_2/Fe(II) oxidation; ROSs yield; *In situ* chemical oxidation

1. Introduction

Due to the instability of liquid H_2O_2 in the subsurface, the use of the conventional Fenton reaction for in situ remediation applications is limited. This has led to the development of

*Corresponding author: Tel: +86 21 64250709, Fax: +86 21 64252737, suiqian@ecust.edu.cn (Q. Sui), lvshuguang@ecust.edu.cn (S. Lyu).

stable H_2O_2 sources for subsurface applications. It has been reported that calcium peroxide (CaO_2) can produce H_2O_2 over a wide pH range (Eq. 1).

$$CaO_2 + H_2O \rightarrow Ca(OH)_2 + H_2O_2 \quad (1)$$

As a solid, not all of the contained H_2O_2 is available at once. Hence, the slow release of H_2O_2 from CaO_2 can reduce unexpected H_2O_2 loss, making CaO_2 a more effective source of H_2O_2 than liquid H_2O_2. For example, Northup and Cassidy [1] reported that CaO_2 was a more efficient oxidant than liquid H_2O_2 at pHs greater than 6 for the treatment of tetrachloroethene. Similarly, Bogan et al. [2] found that the removal efficiency was enhanced from 5% to 44% after the substitution of H_2O_2 with CaO_2 in the treatment of polycyclic aromatic hydrocarbons (PAHs). Moreover, CaO_2 has been used in removing endocrine disrupting compounds, cable insulating oil, toluene, trichloroethylene, benzene, and other organics [3–7]. The treatment process using CaO_2 alone is relatively inefficient, and the introduction of Fe(II) can greatly accelerate the process [6,7].

Prior research has reported that hydroxyl radical ($HO^{\bullet}$) and superoxide radical anions ($O_2^{\bullet-}$) as the probable reactive oxygen species (ROSs) produced in CaO_2 based oxidation systems [5–9]. However, many of the reported results were deduced from degradation performance rather than specific testing of radical generation. Thus, the specific generation of ROSs and the influence of system conditions on ROSs yield is still unclear. In addition, several factors common to oxidation experiments can obscure the identification and quantification of ROSs. First, it is possible that intermediate radicals may also contribute to contaminant degradation [10]. Second, the presence of other constituents, such as catalysts, salts, co-contaminants, degradation intermediaries, and dissolved organic carbon, can compete with the target compound for the ROSs [6,7,9–12]. Although the degradation performance can provide information about the primary ROS involved, the results are uncertain. So far, there are few studies focusing on the generations of these ROSs in the CaO_2 based Fenton system, particularly regarding generation efficiency of $HO^{\bullet}$. Such information is required to support the efficient use of ROSs in the CaO_2/Fe(II) Fenton system. Thus it is critical to design experiments specifically for evaluating the generation of $HO^{\bullet}$ and $O_2^{\bullet-}$ and investigating the influence of solution chemistry to improve our understanding of the CaO_2/Fe(II) Fenton system for application to contamination remediation.

The radical-specific probe analysis approach can be used to characterize radical generation [13–15]. For $HO^{\bullet}$, the frequently used probe compounds include coumarin [16–18], salicylic acid [19–21], benzoic acid (BA) [14,22], 1-propanol [22], and their reaction rate constants with $HO^{\bullet}$ are listed in Table 1 [22]. Conversely, luminol [24,25], methoxy cypiridina luciferin analog (MCLA) [26], and various tetrazolium salts including nitroblue tetrazolium (NBT) [27–29] and 2,3-bis (2-methoxy-4-nitro-5-sulfophenyl)-2H-tetrazolium-5-carboxanilide (XTT) [30] have been used in determining $O_2^{\bullet-}$ generation in various systems. The advantages and disadvantages of the probes in $O_2^{\bullet-}$ determination are also listed in Table 1.

In this study, BA is used as a probe to study the generation of $HO^{\bullet}$ in the CaO_2/Fe(II) Fenton system. It is reported that the reaction between BA and $HO^{\bullet}$ produces p-hydroxybenzoic acid (p-HBA), o-HBA, m-HBA, and other products (Eq. 2).

$$HO^{\bullet} + BA \rightarrow \text{p-HBA} + \text{o-HBA} + \text{m-HBA} + \text{other products} \quad (2)$$

Zhou and Mopper [14] reported that p-, o- and m-HBA accounted for 90 ± 5% of the products from the reaction between $HO^{\bullet}$ and BA. They also found that the detected sensitivity of p-HBA is higher than other isomers, and that it can be used for the calculation of $HO^{\bullet}$ generation with the conversion factor of 5.87 ± 0.18. This method has been employed to quantify $HO^{\bullet}$ generated in Fenton systems [22,31] and other advanced oxidation processes (AOPs) [16,32–35]. However, it should be noted that $HO^{\bullet}$ radicals will react with not only BA, but also other substances such as iron ions, residual H_2O_2, $HO^{\bullet}$ radicals. In other words, the measured $HO^{\bullet}$ is the cumulative capability for production and consumption of $HO^{\bullet}$ in the CaO_2/Fe(II) Fenton system at the sampling point. Furthermore, the expected concentration of p-HBA can be too low to proceed for further oxidation with $HO^{\bullet}$, showing the advantage of this technique in $HO^{\bullet}$ quantification. Therefore, p-HBA can be applicable as an indicator to represent $HO^{\bullet}$ generation capability and be helpful to compare the degradation potentials of the CaO_2/Fe(II) Fenton process in different operating conditions.

NBT does not react with H_2O_2 and $HO^{\bullet}$, and has good selectivity in $O_2^{\bullet-}$ determination and can be used in evaluating $O_2^{\bullet-}$ even at low concentration [27]. Thus, NBT is used to study $O_2^{\bullet-}$ generation in the CaO_2/Fe(II) Fenton system (Eq. 3).

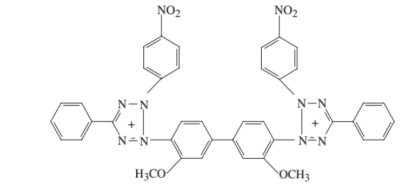

(NBT) + $4O_2^{\bullet-}$ + $2H^+$ →

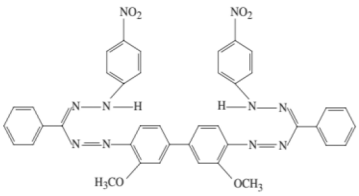

(Formazan)

(3)

NBT can be reduced by $O_2^{\bullet-}$ forming insoluble formazan in aqueous solution, and formazan can be soluble in some aprotic solvents forming a purple solution [5,8]. In addition, the determination of $O_2^{\bullet-}$ can be confirmed by the absorbance of residual NBT solution or the formation of formazan, as shown in Table 1. Ma et al. used NBT to identify

the generation of $O_2^{\bullet-}$ in the CaO_2 system [8], and Qian et al. used NBT to determine $O_2^{\bullet-}$ variation in a nano-CaO_2 system [5]. Although this method cannot quantify $O_2^{\bullet-}$ yield, the results can provide comparable $O_2^{\bullet-}$ concentration and characterize $O_2^{\bullet-}$ variations as a function of experimental design.

Hence, in this study, we use the two above mentioned probes to study the ROSs produced in the CaO_2/Fe(II) system. This supports the deduction of the ROSs generation pathways. Based on the results, we propose an efficient strategy to enhance the $HO^{\bullet}$ generation in the CaO_2 based Fenton system.

2. Experiments

2.1 Experimental design

All experiments were performed in 250 mL glass vessels with a jacket for temperature control at 20 ± 2°C. The materials used are listed in Supplementary Material (Text S1).

For $HO^{\bullet}$ determination, a single dose of CaO_2 and Fe(II) was added to BA solution with vigorous mixing. Control tests with the absence of CaO_2 or Fe(II) were carried out in parallel. 2 mL samples were taken at the predetermined time and quenched by 0.1 mL 1-propanol, and followed by pH adjustment for reducing p-HBA loss in the filter. The treated samples were then acidized and analyzed by the high performance liquid chromatography (HPLC) to quantify $HO^{\bullet}$ generation through p-HBA production between BA and $HO^{\bullet}$ [18].

To evaluate $O_2^{\bullet-}$, a single dose of CaO_2 and Fe(II) was added in ultrapure water with vigorous mixing. 5 mL samples were taken at the predetermined time and immediately mixed with 5 mL NBT solution [5]. The precipitant was dissolved in 5 mL ethanol, and then the organic phase was measured with DR-6000 spectrophotometer (HACH, USA).

BA and NBT solutions were equilibrated with ultrapure water. The fresh probe solutions were prepared daily. All the experiments were conducted twice and the mean values were presented.

2.2 Analytical methods

Analyses of BA and p-HBA were conducted by using an HPLC (Shimadzu LC-20AT, Japan) coupled with UV–vis detector (SPD-20A) and an auto-sampler (SIL-20A). A 10 μL sample was injected into ODS-SP reversed-phase column (5 μm, 4.6 mm × 250 mm). The isocratic eluent was a solvent mixture of 0.1% phosphoric acid (v/v) (A) and methanol (B), and the flow rate was 1.0 mL min^{-1}. p-HBA was quantified at 255 nm, and BA was quantified at 225 nm [18]. Both BA and p-HBA were stable during the whole analyses. In order to reduce the loss of BA and p-HBA, NaOH was used to raise the sample pH > 8 before filtering a 0.22 μm nylon filter (Aladdin, China), and the filtered solution was adjusted to pH 3 via H_2SO_4 [20]. NBT-formazan was analyzed by spectrophotometer (DR-6000, HACH, USA) under the wavelength scanning mode. Ultrapure water was obtained from Class DI purification system (ELGA, 102 Marlow, UK).

H_2O_2 was determined by spectrophotometric method [36], and the concentration of the available Fe(II) was determined according to the modified 1,10-phenanthroline method [37,38]. The solution pH was recorded by a pH meter equipped with a pH/ATC electrode (Sartorius, PB-10, Germany).

3. Results and Discussion

3.1 $HO^{\bullet}$ generation in the CaO_2/Fe(II) Fenton system

The major $HO^{\bullet}$ source in the CaO_2/Fe(II) Fenton system is derived from the reactions as shown in Eqs. 1 and 4. There are also several reactions occurring simultaneously that act as $HO^{\bullet}$ sinks (Eqs. 5–7). Fig. S1 shows the fate of $HO^{\bullet}$ in the presence of BA in the CaO_2/Fe(II) Fenton system. Due to the various sinks, a high concentration of probe is required in this study, and the reaction between $HO^{\bullet}$ and the probe compound should be dominant, ensuring the reaction mirrors $HO^{\bullet}$ generation [39].

$$Fe^{2+} + H_2O_2 \rightarrow Fe^{3+} + HO^- + HO^{\bullet} \quad (4)$$

$$HO^{\bullet} + H_2O_2 \rightarrow HO_2^{\bullet} + H_2O \quad (5)$$

$$HO^{\bullet} + Fe^{2+} \rightarrow Fe^{3+} + OH^- \quad (6)$$

$$HO^{\bullet} + HO^{\bullet} \rightarrow H_2O_2 \quad (7)$$

The results of preliminary tests are shown in the Supplementary Material (Text S2, Fig. S2). Fig. S2a shows that $HO^{\bullet}$ generation increased with increasing BA concentration, and Figs. S2b and 2c present the residual BA concentration. Fig. S3 displays the HPLC chromatograms of the p-HBA and BA when the molar ratio of CaO_2/Fe(II)/BA was set at 1/1/10, which was selected as the control condition in the followed experiments. The results demonstrate that BA is a suitable probe compound for quantifying $HO^{\bullet}$ in the CaO_2/Fe(II) system, and the BA concentration is optimized and selected as 10 mM to trap $HO^{\bullet}$ in the following experiments.

3.1.1 The roles of CaO_2 and Fe(II) on $HO^{\bullet}$ generation—The control tests showed that CaO_2 or Fe(II) alone could not react with BA to generate p-HBA (Fig. 1), and that the reaction between CaO_2 and Fe(II) is the main source for $HO^{\bullet}$ generation. Thus both CaO_2 and Fe(II) are the crucial factors affecting $HO^{\bullet}$ yield.

Fig. 1 illustrates the effect of CaO_2 dosage on $HO^{\bullet}$ generation. The experiments were carried out with the varied CaO_2 dosage from 0 to 4.0 mM, whilst fixing the initial Fe(II) concentration at 1.0 mM. Since $HO^{\bullet}$ originated from the CaO_2/Fe(II) Fenton reaction, it was expected that the amount of $HO^{\bullet}$ would proportionally increase with the increased dosage of CaO_2. As shown in Fig. 2, it is clear that the amount of $HO^{\bullet}$ increased 2.9 fold when CaO_2 concentration increased from 0.5 to 2.0 mM, and the depletion rate of Fe(II) was simultaneously increased from 0.069 to 0.085 mM min^{-1} in the first 10 mins, and the production of $HO^{\bullet}$ was accordingly enhanced. However, further increasing CaO_2 concentration to 4.0 mM had less benefit to the generation of $HO^{\bullet}$. Though the depletion rate of Fe(II) was slightly increased from 0.085 to 0.087 mM min^{-1} in the first 10 mins, the detected H_2O_2 was doubled with a doubled CaO_2 dosage of 4.0 mM (Fig. 2a). The excessive H_2O_2 would also act as $HO^{\bullet}$ sink which competed with BA for reaction with $HO^{\bullet}$ (Eq. 5). Therefore, too much CaO_2 could cause more useless $HO^{\bullet}$ scavenging and less $HO^{\bullet}$ production. Besides, the initially added Fe(II) will be oxidized to Fe(III) within minutes and thereafter the Fenton system will performance independent of the added Fe(II) presenting an initial burst of $HO^{\bullet}$ [40–42].

Because $HO^{\bullet}$ originated from H_2O_2 decomposition catalyzed by Fe(II), Fe(II) dosage should have great influence on $HO^{\bullet}$ generation. Fig. 1 shows the increase in $HO^{\bullet}$ concentration from 0.29 to 0.32 mM after 60 min reaction when Fe(II) dosage increased from 0.5 to 1.0 mM. However, further increasing Fe(II) dosage to 4.0 mM reduced the generation of $HO^{\bullet}$ to 0.24 mM. Figs. 2c and 2d show the changes of H_2O_2 and Fe(II). When Fe(II) dosage was 0.5 and 1.0 mM, H_2O_2 increased in the initial 10 min and later declined significantly (Fig. 2c). It is noted that the variation of Fe(II) was quite different. With the increase of Fe(II) dosage, the consumption of Fe(II) rapidly rose in the initial 10 min and then exhibited a plateau (Fig. 2d). Further increasing Fe(II) dosage over 2.0 mM resulted in a different pattern. The consumption of Fe(II) was observed within the initial 5 min, while H_2O_2 was not detected at the very beginning of the reaction (Fig. 2c). The rapid consumption of Fe(II) and H_2O_2 indicates fast reactions, which could lead to a dramatic increase in $HO^{\bullet}$ generation in a short time. However, the reaction between $HO^{\bullet}$ and Fe(II) can scavenge $HO^{\bullet}$ leading to a low $HO^{\bullet}$ yield (Eq. 6), and the rapid generation of $HO^{\bullet}$ can also favor radical-radical reactions over radical-organic reactions, therefore limiting the detection of the generated radicals [11]. Fig. 2d shows when the molar ratios of CaO_2/Fe(II) were 1/2 and 1/4, the consumed Fe(II) was 60% and 30%, respectively. The similar consumption of Fe(II) and H_2O_2 led to a comparable $HO^{\bullet}$ generation, and as a result, the actual generation of $HO^{\bullet}$ was similar in these two CaO_2/Fe(II) molar ratio conditions.

The above results showed that too much CaO_2 or Fe(II) does not benefit $HO^{\bullet}$ generation, and that the $HO^{\bullet}$ yield depends on an optimal molar ratio of CaO_2/Fe(II), which is consistent with previous reports [3–7]. However, our results further indicated that the $HO^{\bullet}$ generation efficiency was more sensitive to the changes of CaO_2 compared to that of Fe(II). Fixing Fe(II) at 1 mM, the $HO^{\bullet}$ generation efficiency decreased from 34% to 6% when the initial CaO_2 dosage increased from 0.5 to 4 mM (Table 2). In contrast, the $HO^{\bullet}$ generation efficiency decreased from 38% to 26% when the initial Fe(II) dosage increased from 0.5 to 4 mM when fixing CaO_2 at 1 mM (Table 2). The results suggest that regulating Fe(II) could be

more convenient and practical to improve the performance of the CaO_2/Fe(II) system in terms of $HO^{\bullet}$ generation efficiency.

The variation of pH during the experiments was also monitored, and the results showed that the impacts caused by the reagents were different (Table 2). The ΔpH (ΔpH = final pH - initial pH) increased with the increase of CaO_2 dosage, while slight changes in ΔpH were found when varying Fe(II) from 0.5 to 4.0 mM. However, the ΔpH range was limited (ΔpH < 1) in most experiments except for CaO_2/Fe(II) molar ratio of 4/1. The solution pH increased with increasing CaO_2 dosage, with pH greater than 5.0 when 4.0 mM CaO_2 was applied. This increase in pH suppressed the Fenton reaction. Hence, it is necessary to further clarify the effect of pH on $HO^{\bullet}$ generation.

3.1.2 Effect of solution pH on $HO^{\bullet}$ formation—

Fig. 3a illustrates the effect of the initial solution pH (without buffer) on $HO^{\bullet}$ generation. With the pH elevation from 3 to 10, the detected $HO^{\bullet}$ decreased from 0.36 to 0.018 mM. $HO^{\bullet}$ yield significantly declined with the increase of solution pH (Fig. 3b). The results suggest that an acidic environment is more favorable to $HO^{\bullet}$ generation in the CaO_2/Fe(II) system, and this trend is consistent with the general observation in Fenton reactions in which the optimum solution pH value for Fenton oxidation process is approximately 3.

It is obvious that the majority of Fe(II) was consumed in a short time (Fig. 3c), and p-HBA generation was rapid subsequent to the $HO^{\bullet}$ surge. When the initial pH > 4, Fe(II) dropped sharply (Fig. 3c) and the shortage of Fe(II) can limit $HO^{\bullet}$ generation. Fig. 3d shows that for pH ≤ 4 the monitored H_2O_2 increased sharply, after which the residual H_2O_2 declined steadily as a single-peak curve. However, different H_2O_2 patterns were observed when the pH > 4. Less H_2O_2 was detected at the very beginning of the reaction when pH = 5.5 ~ 10 (Fig. 3d). Northup and Cassidy [1] reported that the increase of solution pH would lower the dissolution rate of CaO_2 and H_2O_2 yields; meanwhile, the rapid consumption of Fe(II) in the beginning exacerbated the exhaustion of H_2O_2 from CaO_2. Therefore, although $HO^{\bullet}$ rose sharply, H_2O_2 was not detected in the beginning when pH > 4. The monitored H_2O_2 then increased markedly and presented moderate downward trends in the following period when pH > 4, and the residual H_2O_2 was obviously higher because of the insignificant H_2O_2 decomposition as a result of Fe(II) shortage. This behavior differs greatly from the results when pH < 4 (Fig. 3d). In addition, the generation of $HO^{\bullet}$ in the CaO_2 based system at neutral and alkaline pH conditions was deduced based on contaminant degradation behavior in previous studies [3,5–7]. The detected p-HBA in this study provides direct evidence that $HO^{\bullet}$ is generated in the CaO_2/Fe(II) system at neutral and alkaline pH conditions (Fig. 3b).

3.2 $O_2^{\bullet-}$ generation in the CaO_2/Fe(II) Fenton system

Besides $HO^{\bullet}$, $O_2^{\bullet-}$ is another possible ROS involved in the CaO_2 based system. $O_2^{\bullet-}$ propagation and termination in Fenton reactions are presented by Eqs. 8 ~ 12.

$$HO^{\bullet} + H_2O_2 \rightarrow H_2O + HO_2^{\bullet} \leftrightarrow O_2^{\bullet -} + H_2O + H^{+} \quad (8)$$

$$Fe^{3+} - complex + H_2O_2 \rightarrow Fe^{2+} - complex + O_2^{\bullet -} + 2H^+ \quad (9)$$

$$HO^{\bullet} + O_2^{\bullet -} + H^+ \rightarrow H_2O_2 + O_2 \quad (10)$$

$$2O_2^{\bullet -} + 2H^+ \rightarrow H_2O_2 + O_2 \quad (11)$$

$$Fe^{3+} - complex + O_2^{\bullet -} \rightarrow Fe^{2+} - complex + O_2 \quad (12)$$

$$e^- + H_2O_2 \rightarrow HO^- + HO^{\bullet} \quad (13)$$

Based on Eq. 3, NBT was used to capture $O_2^{\bullet -}$ produced in the CaO_2 based system, and the preliminary study confirmed $O_2^{\bullet -}$ was produced in the CaO_2/Fe(II) Fenton system (Supplementary Material, Text S3, Fig. S4).

The effects of CaO_2 and Fe(II) dosage on $O_2^{\bullet -}$ production were investigated. The results indicate that $O_2^{\bullet -}$ production increased with the CaO_2 dosage, but $O_2^{\bullet -}$ variations were not strictly proportional to CaO_2 dosage (Supplementary Material, Text S4, Fig. S5a). Fig. S6 suggests that $O_2^{\bullet -}$ can be produced through different pathways. For the CaO_2 based Fenton system, $O_2^{\bullet -}$ can be produced by the Fenton pathway through various reactions as a result of H_2O_2 decomposition (Eqs. 8 ~ 12). The results in Fig. S6 also indicate that $O_2^{\bullet -}$ can be generated via a non-Fenton pathway wherein CaO_2 reacts with water (Eqs. 13, 8 & 9) [8,42,43]. Too much CaO_2 can depress the Fenton-pathway based $O_2^{\bullet -}$ generation but has less influence on the non-Fenton pathway $O_2^{\bullet -}$ generation (Supplementary Material, Text S4) [8].

In contrast, too much Fe(II) can produce more Fe(III), and the increase of Fe(III) can increase $O_2^{\bullet -}$ scavenging, leading to low $O_2^{\bullet -}$ yield (Fig. S5b). Moreover, the decline of $HO^{\bullet}$ also constrained $O_2^{\bullet -}$ generation pathways. The influence of initial solution pH (from 3 to 10) on $O_2^{\bullet -}$ generation was also studied. The lowest $O_2^{\bullet -}$ peak was observed at pH = 3 when the highest $HO^{\bullet}$ yield was observed. The absorbance was even slightly enhanced when increasing pH to 10 (Supplementary Material, Text S5, Fig. S7), suggesting that the alkaline solution pH could be efficient in encouraging $O_2^{\bullet -}$ generation.

3.3 ROS generation mechanism in the CaO_2/Fe(II) system

Based on the experimental results, the proposed mechanism of ROSs generation in the CaO_2/Fe(II) system is displayed in Fig. 4.

The CaO_2 dissolution process in water is slow, but the dissolved CaO_2 can rapidly produce H_2O_2 in aqueous solution [43]. The addition of Fe(II) initiates the Fenton reaction. Fe(II) reacts with the produced H_2O_2 to generate $HO^{\bullet}$ and $O_2^{\bullet-}$, which are confirmed by the p-HBA generation and NBT tests, respectively. The produced H_2O_2 can possibly obtain an electron leading to the non-Fenton pathway which can generate $HO^{\bullet}$ and $O_2^{\bullet-}$ [5,8]. Compared with the non-Fenton pathway, the Fenton pathway is the major reactive species source, and $HO^{\bullet}$ is the primary radical in the CaO_2/Fe(II) system. The molar ratio of CaO_2/Fe(II) can change the performance of the Fenton reactions, resulting in different radicals distribution. The solution pH can affect CaO_2 dissolution performance, thereby altering H_2O_2 release and lead to different radical yields.

3.4 New strategy for the enhancement of $HO^{\bullet}$ formation

Due to its reactive properties of non-selectivity and high efficiency with most organic contaminants, $HO^{\bullet}$ is the key reactive species in the CaO_2/Fe(II) system. Based on the prior analysis, pH and the molar ratio of CaO_2/Fe(II) can influence the $HO^{\bullet}$ generation efficiency. However, pH adjustment is difficult to implement for subsurface systems and requires additional acid chemicals. Thus, regulating the molar ratio of CaO_2/Fe(II) is the easier, more effective way to optimize $HO^{\bullet}$ generation efficiency. Since rapid $HO^{\bullet}$ generation can constrain $HO^{\bullet}$ efficiency, it is necessary to study if moderate reaction benefits more $HO^{\bullet}$ generation. CaO_2 is stable and can release H_2O_2 for a relatively long time [1,43], and the dosage of Fe(II) has the potential to affect the $HO^{\bullet}$ yield. Hence, Fe(II) could be the more suitable factor regulating $HO^{\bullet}$ generation (Supplementary Material, Text S6). Changing Fe(II) dosing method from the single dose to sequential addition might be an option to optimize $HO^{\bullet}$ generation, which can constrain the competition reactions.

After two-step additions of Fe(II) (0.5 mM for each time), the final molar ratio of CaO_2/Fe(II) reached 1/1, and the overall $HO^{\bullet}$ was 0.41 mM (Fig. 5a). It is noted that $HO^{\bullet}$ generation was significantly accelerated after the second dosing of Fe(II), and the two-step additions of Fe(II) also improved $HO^{\bullet}$ generation by 14% in comparison to the same final concentration of CaO_2/Fe(II) (single step addition of Fe(II)). This test demonstrates that is feasible to control $HO^{\bullet}$ generation by varying the Fe(II) dosing method.

An additional experiment test was conducted to further test this hypothesis, in which Fe(II) solution was transferred successively within 120 min by a persist pump to the reactor containing a CaO_2/BA molar ratio of 1/10 and reaching the final molar ratio of CaO_2/Fe(II) = 1/1. With the successive addition of Fe(II), $HO^{\bullet}$ was steadily generated in the CaO_2/Fe(II) system, and in this situation $HO^{\bullet}$ generation presented a curve which was similar to the change of Fe(II) amount but different from other $HO^{\bullet}$ generation curves (Fig. 5a and 5b). This result showed that $HO^{\bullet}$ generation can be manipulated by successively dosing Fe(II), and the final $HO^{\bullet}$ was increased to 0.49 mM, representing an increase of 37% in $HO^{\bullet}$ generation.

The changes of Fe(II) and H_2O_2 during the course of sequential addition of Fe(II) are given in Figs. 5b and 5c. In the two-step additions of Fe(II) test, the value of Fe(II) exhibited a stepwise increase, while H_2O_2 presented a sharp drop when the other half Fe(II) was added to the reactor. The trends in the successive addition of Fe(II) test were completely different. With a continuous increment of Fe(II), the available Fe(II) rose moderately, and H_2O_2 dramatically increased and then steadily dropped as a single-peak curve. The lower Fe(II) concentration, the same final H_2O_2 concentration as well as the higher $HO^{\bullet}$ generation indicated that the reaction was successfully tuned by gradually dosing Fe(II). The successively dosing Fe(II) contributed to a slow and steady production of $HO^{\bullet}$, and played an important role in the CaO_2/Fe(II) system. It was obvious that successively providing Fe(II) could decrease $HO^{\bullet}$ generation rate, and the generated $HO^{\bullet}$ would prefer to react with BA [11]. In addition, the scavenging of $HO^{\bullet}$ by Fe(II) and $HO^{\bullet}$ self-reaction were also limited, hence resulted in a higher $HO^{\bullet}$ generation [11,43]. Therefore, combing the successive dosing of Fe(II) with the application of CaO_2 can be a more efficient and convenient strategy to treat contamination.

This strategy has implications for using *in situ* chemical oxidation employing CaO_2 to treat contaminated groundwater. A possible application scheme and model is shown in Fig. 6. In the injection and transport steps, after dosing the proper conditioning reagents, CaO_2 slurry is first injected into the contaminated groundwater, spreading into the contamination zone. Then the treatment process can be regulated by injecting Fe(II) solution. When Fe(II) is periodically pumped into the zone, Fe(II) starts the Fenton reaction, and can also decrease the solution pH and accelerate H_2O_2 generation, which benefits the Fenton process. When the contaminant is completely oxidized, the reaction can be halted by stopping injection of Fe(II) solution. However, the groundwater flow and background solution matrix are different from the experimental conditions, which may affect CaO_2 migration, H_2O_2 generation, and the Fenton reaction efficiency (Supplementary Material, Fig. S8). And the influence of CaO_2 based Fenton system on the groundwater ecosystem is another concern, which requires more investigation in the future.

4. Conclusion

The generation of ROSs in the CaO_2/Fe(II) system was investigated. BA and NBT were applied as probe compounds to capture the generated $HO^{\bullet}$ and $O_2^{\bullet-}$, respectively. For $HO^{\bullet}$, the CaO_2 based Fenton reaction was the main source, and the dosage of CaO_2 and Fe(II) greatly affected $HO^{\bullet}$ generation, suggesting an optimal molar ratio of CaO_2/Fe(II) was required for optimization of $HO^{\bullet}$ yield. The CaO_2/Fe(II) system favored the acidic environment in terms of $HO^{\bullet}$ generation. For CaO_2 based Fenton system, $O_2^{\bullet-}$ can be produced through various reactions initiated by Fe(II) and H_2O_2 forming Fenton pathway, and can also be directly generated when CaO_2 reacts with water developing a non-Fenton pathway. The $O_2^{\bullet-}$ generation was more sensitive to the CaO_2 dosage. The influence of solution pH on $O_2^{\bullet-}$ generation was different from that on $HO^{\bullet}$. The sequential dosing of Fe(II) can be an efficient strategy to generate higher $HO^{\bullet}$ in the CaO_2/Fe(II) system, showing a potential application of this technique for groundwater remediation.

Supplementary Material

Refer to Web version on PubMed Central for supplementary material.

Acknowledgement

This study was financially supported by the grant from the National Natural Science Foundation of China (41373094), Natural Science Foundation of Shanghai, China (16ZR1407200). The contributions of Mark Brusseau were supported by the NIEHS Superfund Research Program (PS 42 ES04940).

Reference

[1]. Northup A, Cassidy D, Calcium peroxide (CaO2) for use in modified Fenton chemistry, J. Hazard. Mater 152 (2008) 1164–1170. doi:10.1016/j.jhazmat.2007.07.096. [PubMed: 17804164]

[2]. Bogan BW, Trbovic V, Paterek JR, Inclusion of vegetable oils in Fenton's chemistry for remediation of PAH-contaminated soils, Chemosphere. 50 (2003) 15–21. doi:10.1016/S0045-6535(02)00490-3. [PubMed: 12656224]

[3]. Zhang A, Wang J, Li Y, Performance of calcium peroxide for removal of endocrine-disrupting compounds in waste activated sludge and promotion of sludge solubilization, Water Res. 71 (2015) 125–139. doi:10.1016/j.watres.2015.01.005. [PubMed: 25613412]

[4]. Xu J, Pancras T, Grotenhuis T, Chemical oxidation of cable insulating oil contaminated soil, Chemosphere. 84 (2011) 272–277. doi:10.1016/j.chemosphere.2011.03.044. [PubMed: 21571353]

[5]. Qian Y, Zhou X, Zhang Y, Zhang W, Chen J, Performance and properties of nanoscale calcium peroxide for toluene removal, Chemosphere. 91 (2013) 717–723. doi:10.1016/j.chemosphere.2013.01.049. [PubMed: 23466092]

[6]. Zhang X, Gu X, Lu S, Miao Z, Xu M, Fu X, Qiu Z, Sui Q, Degradation of trichloroethylene in aqueous solution by calcium peroxide activated with ferrous ion, J. Hazard. Mater 284 (2015) 253–260. doi:10.1016/j.jhazmat.2014.11.030. [PubMed: 25463240]

[7]. Xue Y, Gu X, Lu S, Miao Z, Brusseau ML, Xu M, Fu X, Zhang X, Qiu Z, Sui Q, The destruction of benzene by calcium peroxide activated with Fe(II) in water, Chem. Eng. J 302 (2016) 187–193. doi:10.1016/j.cej.2016.05.016. [PubMed: 28943778]

[8]. Ma Y, Zhang B, Zhao L, Guo G, Lin J, Study on the generation mechanism of reactive oxygen species on calcium peroxide by chemiluminescence and UV-visible spectra, Luminescence. 22 (2007) 575–580. doi:10.1002/bio. [PubMed: 17768715]

[9]. Lu S, Zhang X, Xue Y, Application of calcium peroxide in water and soil treatment: A review, J. Hazard. Mater 337 (2017) 163–177. doi:10.1016/j.jhazmat.2017.04.064. [PubMed: 28525879]

[10]. Xue Y, Lu S, Fu X, Sharma VK, Mendoza-Sanchez I, Qiu Z, Sui Q, Simultaneous removal of benzene, toluene, ethylbenzene and xylene (BTEX) by CaO2 based Fenton system: Enhanced degradation by chelating agents, Chem. Eng. J 331 (2018) 255–264. doi:10.1016/j.cej.2017.08.099.

[11]. Peyton GR, The free radical chemistry of persulfate based total organic carbon analyzers, Mar. Chem 41 (1993) 91–103. doi:10.1016/0304-4203(93)90108-z.

[12]. Liang C, Bruell CJ, Marley MC, Sperry KL, Persulfate oxidation for in situ remediation of TCE. I. Activated by ferrous ion with and without a persulfate-thiosulfate redox couple, Chemosphere. 55 (2004) 1213–1223. doi:10.1016/j.chemosphere.2004.01.029. [PubMed: 15081762]

[13]. Mwebi NO, FENTON & FENTON-LIKE REACTIONS: NATURE OF OXIDIZING INTERMEDIATES, 2005 http://drum.lib.umd.edu/handle/1903/9139.

[14]. Zhou X, Mopper K, Determination of photochemically produced hydroxyl radicals in seawater and freshwater, Mar. Chem 30 (1990) 71–88. doi:10.1016/0304-4203(90)90062-H.

[15]. Fernández-Castro P, Vallejo M, San Román MF, Ortiz I, Insight on the fundamentals of advanced oxidation processes: Role and review of the determination methods of reactive oxygen species, J. Chem. Technol. Biotechnol 90 (2015) 796–820. doi:10.1002/jctb.4634.

[16]. Maezono T, Tokumura M, Sekine M, Kawase Y, Hydroxyl radical concentration profile in photo-Fenton oxidation process: Generation and consumption of hydroxyl radicals during the discoloration of azo-dye Orange II, Chemosphere. 82 (2011) 1422–1430. doi:10.1016/j.chemosphere.2010.11.052. [PubMed: 21146853]

[17]. Tokumura M, Morito R, Hatayama R, Kawase Y, Iron redox cycling in hydroxyl radical generation during the photo-Fenton oxidative degradation: Dynamic change of hydroxyl radical concentration, Appl. Catal. B Environ 106 (2011) 565–576. doi:10.1016/j.apcatb.2011.06.017.

[18]. Lin ZR, Zhao L, Dong YH, Quantitative characterization of hydroxyl radical generation in a goethite-catalyzed Fenton-like reaction, Chemosphere. 141 (2015) 7–12. doi:10.1016/j.chemosphere.2015.05.066. [PubMed: 26069944]

[19]. Tomita M, Okuyama T, Watanabe S, Watanabe H, Quantitation of the hydroxyl radical adducts of salicylic acid by micellar electrokinetic capillary chromatography: Oxidizing species formed by a Fenton reaction, Arch. Toxicol 68 (1994) 428–433. doi:10.1007/s002040050093. [PubMed: 7979959]

[20]. Luo X, Lehotay DC, Determination of hydroxyl radicals using salicylate as a trapping agent by gas chromatography-mass spectrometry, Clin. Biochem 30 (1997) 41–46. doi:10.1016/S0009-9120(96)00137-3. [PubMed: 9056108]

[21]. Goi A, Veressinina Y, Trapido M, Degradation of salicylic acid by Fenton and modified Fenton treatment, Chem. Eng. J 143 (2008) 1–9. doi:10.1016/j.cej.2008.01.018.

[22]. Lindsey ME, Tarr MA, Quantification of hydroxyl radical during Fenton oxidation following a symple addition of iron and peroxide, Chemosphere. 41 (2000) 409–417. [PubMed: 11057603]

[23]. Buxton GV, Greenstock CL, Helman WP, Ross AB, Critical review of rate constants for reactions of hydrated electrons, hydrogen atoms and hydroxyl radicals in aqueous solution, J. Phys. Chem. Ref. Data 17 (1988) 513–886.

[24]. McMurray HN, Wilson BP, Mechanistic and spatial study of ultrasonically induced luminol chemiluminescence, J. Phys. Chem. A 103 (1999) 3955–3962. doi:10.1021/jp984503r.

[25]. Mahé É, Bornoz P, Briot E, Chevalet J, Comninellis C, Devilliers D, A selective chemiluminescence detection method for reactive oxygen species involved in oxygen reduction reaction on electrocatalytic materials, Electrochim. Acta 102 (2013) 259–273. doi:10.1016/j.electacta.2013.03.190.

[26]. Fujimori K, Komiyama T, Tabata H, Nojima T, Ishiguro K, Sawaki Y, Tatsuzawa H, Nakano M, Chemiluminescence of cypridina luciferin analogs. Part 3. MCLA chemiluminescence with singlet oxygen generated by the Retro-Diels-Alder reaction of a naphthalene endoperoxide, Photochem. Photobiol 68 (1998) 143–149. doi:10.1111/j.1751-1097.1998.tb02481.x.

[27]. Goto H, Hanada Y, Ohno T, Matsumura M, Quantitative analysis of superoxide ion and hydrogen peroxide produced from molecular oxygen on photoirradiated TiO_2 particles, J. Catal 225 (2004) 223–229. doi:10.1016/j.jcat.2004.04.001.

[28]. Xu X, Duan X, Yi Z, Zhou Z, Fan X, Wang Y, Photocatalytic production of superoxide ion in the aqueous suspensions of two kinds of ZnO under simulated solar light, Catal. Commun 12 (2010) 169–172. doi:10.1016/j.catcom.2010.09.006.

[29]. Chen CY, Jafvert CT, Photoreactivity of carboxylated single-walled carbon nanotubes in sunlight: Reactive oxygen species production in water, Environ. Sci. Technol 44 (2010) 6674–6679. [PubMed: 20687543]

[30]. Sutherland MW, Learmonth BA, The tetrazolium dyes MTS and XTT provide new quantitative assays for superoxide and superoxide dismutase, Free Radic. Res 27 (1997) 283–289. doi:10.3109/10715769709065766. [PubMed: 9350432]

[31]. G. S and Ananthakrishnan R, Semi-quantitative determination of hydroxyl radicals by benzoic acid hydroxylation: An analytical methodology for photo-Fenton systems, Curr. Anal. Chem 8 (2012) 143–149. doi:10.2174/157341112798472297.

[32]. Tong M, Yuan S, Ma S, Jin M, Liu D, Cheng D, Liu X, Gan Y, Wang Y, Production of abundant hydroxyl radicals from oxygenation of subsurface sediments, Environ. Sci. Technol 50 (2016) 214–221. doi:10.1021/acs.est.5b04323. [PubMed: 26641489]

[33]. Yang XJ, Tian PF, Wang HL, Xu J, Han YF, Catalytic decomposition of H_2O_2 over a Au/carbon catalyst: A dual intermediate model for the generation of hydroxyl radicals, J. Catal 336 (2016) 126–132. doi:10.1016/j.jcat.2015.12.029.

[34]. Zeng Q, Dong H, Wang X, Yu T, Cui W, Degradation of 1, 4-dioxane by hydroxyl radicals produced from clay minerals, J. Hazard. Mater 331 (2017) 88–98. doi:10.1016/j.jhazmat.2017.01.040. [PubMed: 28249183]

[35]. Liu G, Li X, Han B, Chen L, Zhu L, Campos LC, Efficient degradation of sulfamethoxazole by the Fe(II)/HSO5−process enhanced by hydroxylamine: Efficiency and mechanism, J. Hazard. Mater 322 (2017) 461–468. doi:10.1016/j.jhazmat.2016.09.062. [PubMed: 27745962]

[36]. Eisenberg G, Colorimetric Determination of hydrogen peroxide, Ind. Eng. Chem. Anal. Ed 15 (1943) 327–328. doi:10.1021/i560117a011.

[37]. Tamura H, Goto K, Yotsuyanagi T, Nagayama M, Spectrophotometric determination of iron(II) with 1,10-phenanthroline in the presence of large amounts of iron(III), Talanta. 21 (1974) 314–318. doi:10.1016/0039-9140(74)80012-3. [PubMed: 18961462]

[38]. Yuegang Z, Jürg H, Formation of Hydrogen peroxide and depletion of oxalic acid in atmospheric water by photolysis of iron(III)-oxalato complexes, Environ. Sci. Technol 26 (1992) 1014–1022. doi:10.1021/es00029a022.

[39]. Blough NV, Electron paramagnetic resonance measurements of photochemical radical production in humic substances. 1. Effects of oxygen and charge on radical scavenging by nitroxides, Environ. Sci. Technol 22 (1988) 77–82. doi:10.1021/es00166a008. [PubMed: 22195513]

[40]. Chen L, Ma J, Li X, Zhang J, Fang J, Guan Y, Xie P, Strong enhancement on Fenton oxidation by addition of hydroxylamine to accelerate the ferric and ferrous iron cycles, Environ. Sci. Technol 45 (2011) 3925–3930. doi:10.1021/es2002748. [PubMed: 21469678]

[41]. Neyens E, Baeyens J, A review of classic Fenton's peroxidation as an advanced oxidation technique, J. Hazard. Mater 98 (2003) 33–50. doi:10.1016/S0304-3894(02)00282-0. [PubMed: 12628776]

[42]. Pignatello JJ, Oliveros E, MacKay A, Advanced oxidation processes for organic contaminant destruction based on the Fenton reaction and related Chemistry, Crit. Rev. Environ. Sci. Technol 36 (2006) 1–84. doi:10.1080/10643380500326564.

[43]. Wang H, Zhao Y, Li T, Chen Z, Wang Y, Qin C, Properties of calcium peroxide for release of hydrogen peroxide and oxygen: A kinetics study, Chem. Eng. J 303 (2016) 450–457. doi:10.1016/j.cej.2016.05.123.

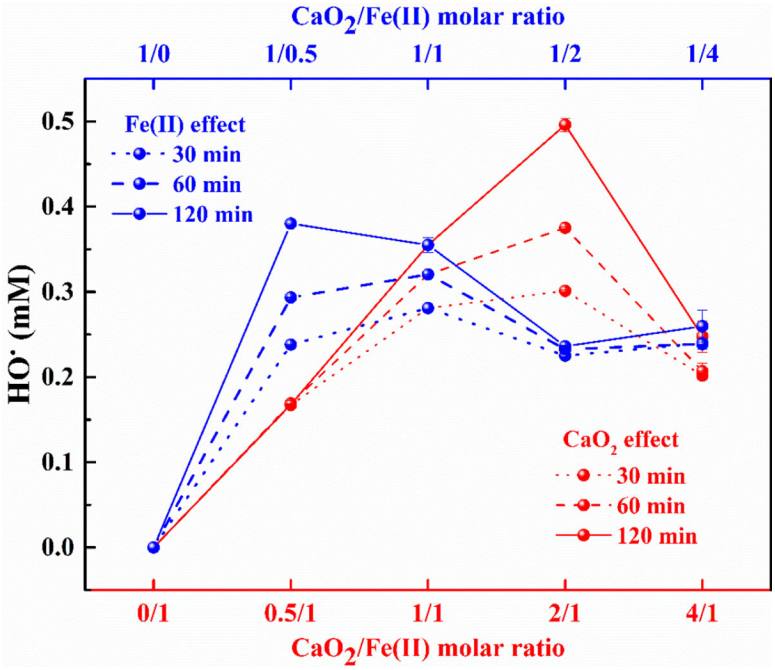

Fig. 1.

(a) The influences of CaO_2 and Fe(II) dosages on $HO^{\bullet}$ generation. (The molar ratios of CaO_2/Fe(II) = 1/0, 1/0.5, 1/1, 1/2, 1/4, 0/1, 0.5/1, 1/1, 2/1, 4/1, **[**$CaO_2]_0$ or $[Fe(II)]_0$ was fixed as 1 mM, $[BA]_0$ =10 mM. $[HO^{\bullet}]$ = 5.87 × [p-HBA]), (b) HPLC chromatograms of the p-HBA and BA. ($[CaO_2]_0 = [Fe(II)]_0$ = 1.0 mM, $[BA]_0$ =10 mM).

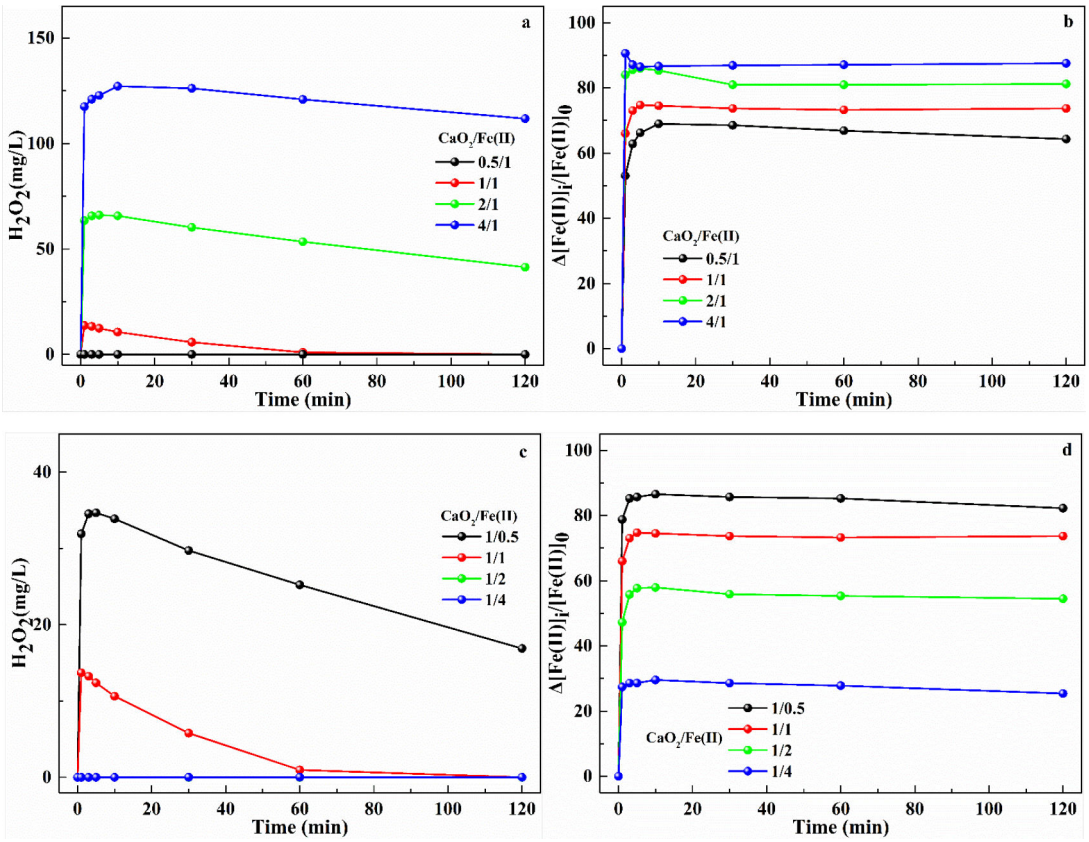

Fig. 2.

The influences of CaO_2 on variations of (a) H_2O_2 and (b) Fe(II) (The molar ratios of CaO_2/Fe(II) = 1/0.5, 1/1, 1/2, 1/4, 0.5/1, 1/1, 2/1, 4/1, $[Fe(II)]_0$ = 1.0 mM, $[BA]_0$ =10 mM); and the influences of Fe(II) on variations of (c) H_2O_2 and (d) Fe(II) (The molar ratios of CaO_2/Fe(II) = 1/0.5, 1/1, 1/2, 1/4, 0.5/1, 1/1, 2/1, 4/1, $[CaO_2]_0$ = 1.0 mM, $[BA]_0$ =10 mM).

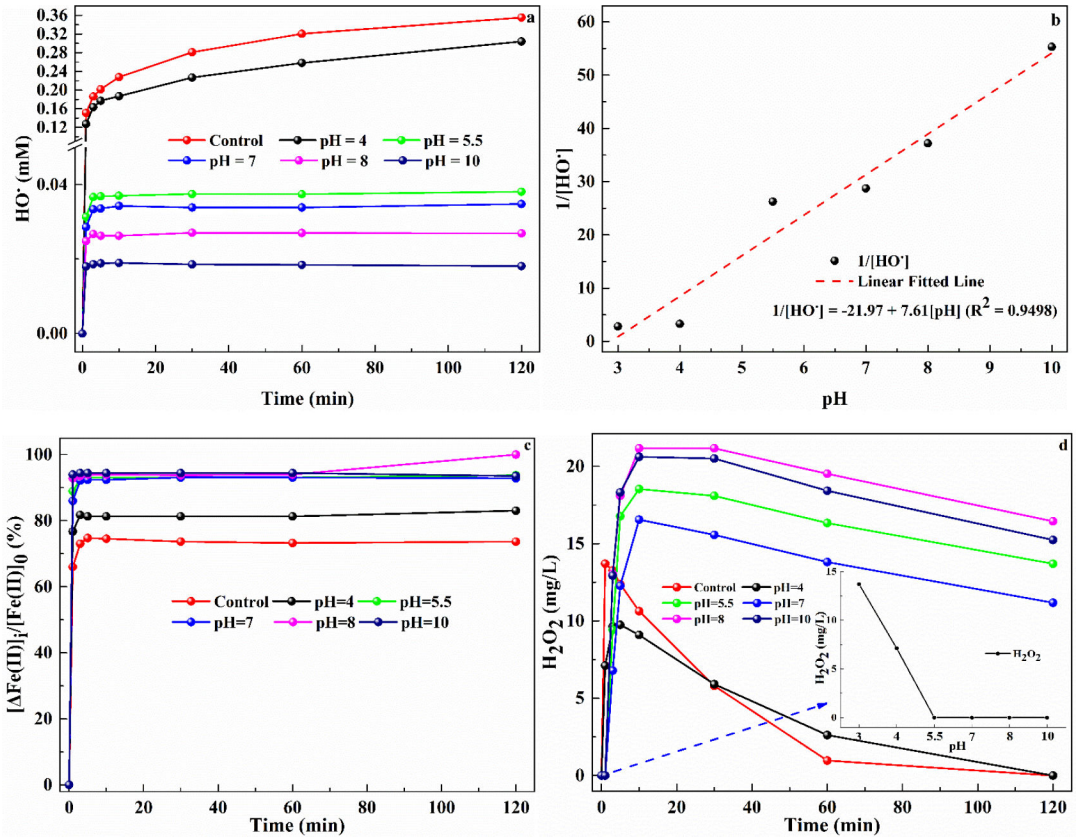

Fig. 3.

(a) The influences of pH on HO● generation, (b) The relationship between pH and HO●; and the influences of pH on changes of (c) Fe(II) and (d) H_2O_2: insert graph: the detected H_2O_2 concentration at 1 min. ($[CaO_2]_0$ = $[Fe(II)]_0$ = 1.0 mM, $[BA]_0$ =10 mM, [HO●] = 5.87 × [p-HBA], the pH of control experiment was 3).

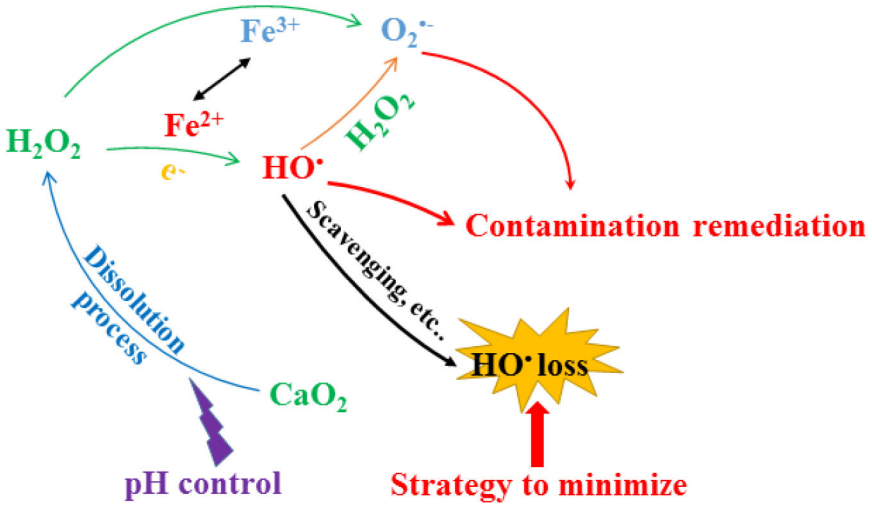

Fig. 4.
The reactive species in the CaO_2/Fe(II) system.

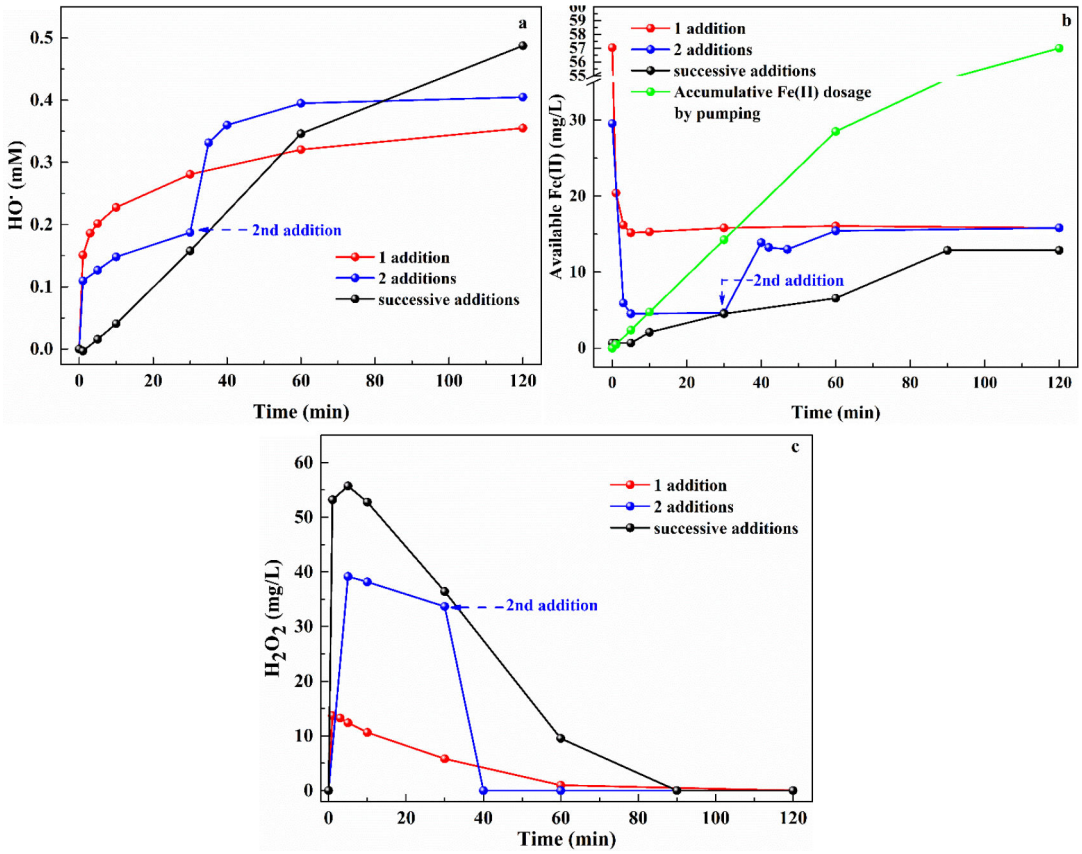

Fig. 5.

The influences of sequential addition of Fe(II) on (a) HO● generation, and (b) variations of available Fe(II) and (c) variations of available H_2O_2. ($[CaO_2]_0 = [Fe(II)]_0 = 1.0$ mM $[BA]_0 = 10$ mM, $[HO^{\bullet}] = 5.87 \times$ [p-HBA]).

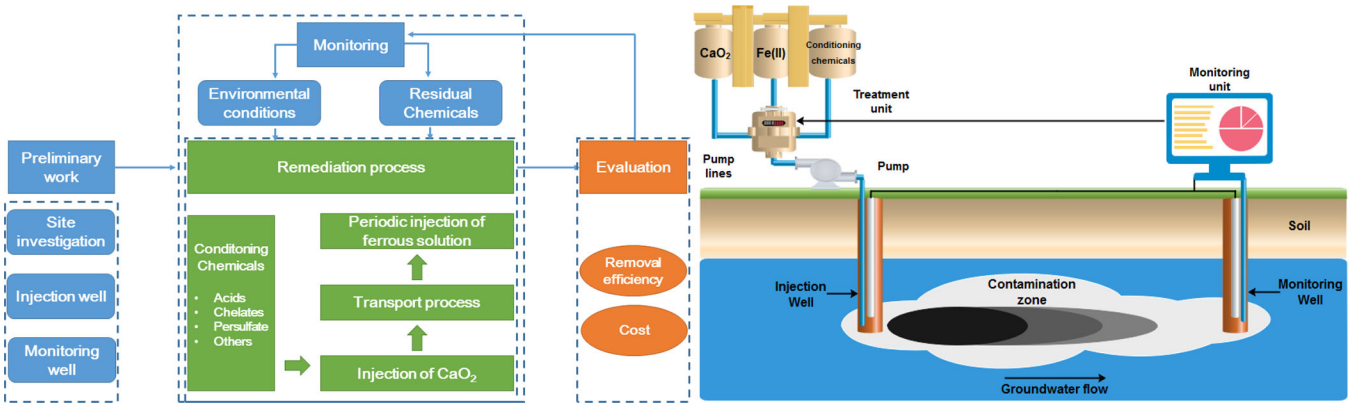

Fig. 6.

Illustration for the possible application of the CaO2/Fe(II) technique.

Table 1

The rate constants for the reactions between probe compounds and $HO^{\bullet}$, and the features of the probe compounds in $O_2^{\bullet-}$ determination

	Probe compound	Reaction	k	Ref.
$HO^{\bullet}$	Coumarin	$C_9H_6O_2 + 2\ HO^{\bullet} \rightarrow C_9H_6O_3 + H_2O$	$6.2 \times 10^9\ M^{-1}\ s^{-1}$	[18]
	Salicylic acid	$C_7H_6O_2 + 2\ HO^{\bullet} \rightarrow C_7H_6O_3$	$5\times 10^9 \sim 5\times 10^{10}\ M^{-1}\ s^{-1}$	[19]
	Benzoic acid	$C_6H_5CO_2H + HO^{\bullet} \rightarrow HOC_6H_5CO_2H$	$5.9 \times 10^9\ M^{-1}\ s^{-1}$	
	1-Propanol	$(CH_3)_2CHOH + HO^{\bullet} \rightarrow C_3H_6O$	$1.9 \times 10^9\ M^{-1}\ s^{-1}$	[23]
	Fe^{2+}	$Fe^{2+} + HO^{\bullet} \rightarrow Fe^{3+} + OH^-$	$4.3 \times 10^8\ M^{-1}\ s^{-1}$	

	Probe compound	Features	Ref.
$O_2^{\bullet-}$	Luminol	Non-selective probes; $O_2^{\bullet-}$ determined by generated chemiluminescence; $pKa_1 = 6.3$, $pKa_2 = 15.21$	[24,25]
	MCLA	Sensitive and wide applicable pH range; $O_2^{\bullet-}$ determined by generated chemiluminescence; $pKa = 7.75$	[26]
	NBT	Not influenced by H_2O_2 and $HO^{\bullet}$; $O_2^{\bullet-}$ determined by the direct absorbance of NBT solution or the indirect absorbance of NBT-formazan; $k(O_2^{\bullet-}) = 5.9 \times 10^4\ M^{-1}\ s^{-1}$	[27–29]
	XTT	Selective and good water solubility; $O_2^{\bullet-}$ determined by the absorbance of XTT solution; $k(O_2^{\bullet-}) = 8.59 \times 10^4\ M^{-1}\ s^{-1}$	[30]

Table 2

$HO^{\bullet}$ initial formation rates, pH variations and pH influence on the $HO^{\bullet}$ yield in the CaO_2/Fe(II) system

	CaO_2/Fe(II)[a]	k[b] (M^{-1} s^{-1})	pH variation[c]	$HO^{\bullet}$ yield[d] (%)
Influence of CaO_2	0.5/1	1.98×10^{-6}	3.01/3.06; 0.05	33.72
	2/1	2.77×10^{-6}	3.05/3.89; 0.84	24.90
	4/1	2.55×10^{-6}	3.08/5.21; 2.13	6.22
	1/1	2.51×10^{-6}	3.07/3.38; 0.31	35.65
Influence of Fe(II)	1/0.5	2.08×10^{-6}	3.05/3.50; 0.45	38.17
	1/2	2.86×10^{-6}	3.07/3.14; 0.07	23.70
	1/4	2.38×10^{-6}	3.09/3.11; 0.02	26.08

	pH	$HO^{\bullet}$ yield[d] (%)
Influence of pH	3	35.65
	4	30.41
	5.5	3.81
	7	3.48
	8	2.69
	10	1.81

a: Molar ratio;

b: Initial rate of $HO^{\bullet}$ formation;

c: Initial pH/Final pH; ΔpH = final pH- initial pH;

d: Based on the theoretical calculation: 0.47 g H_2O_2/g CaO_2, and all the released H_2O_2 participated in Fenton reaction.